



TITLE:

N2O-grown oxides/4H-SiC (0001),  
(0338), and (1120) interface  
properties characterized by using  
p-type gate-controlled diodes

AUTHOR(S):

Noborio, Masato; Suda, Jun; Kimoto, Tsunenobu

---

CITATION:

Noborio, Masato ...[et al]. N2O-grown oxides/4H-SiC (0001), (0338), and (1120) interface properties characterized by using p-type gate-controlled diodes. APPLIED PHYSICS LETTERS 2008, 93(19): 193510.

ISSUE DATE:

2008-11-10

URL:

<http://hdl.handle.net/2433/84573>

RIGHT:

Copyright 2008 American Institute of Physics. This article may be downloaded for personal use only. Any other use requires prior permission of the author and the American Institute of Physics.

# **N<sub>2</sub>O-grown oxides/4H-SiC (0001), (033̄8), and (112̄0) interface properties characterized by using *p*-type gate-controlled diodes**

Masato Noborio,<sup>1,a)</sup> Jun Suda,<sup>1</sup> and Tsunenobu Kimoto<sup>1,2</sup>

<sup>1</sup>*Department of Electronic Science and Engineering, Kyoto University, A1-303 Kyotodaigaku-katsura, Nishikyo, Kyoto 615-8510, Japan*

<sup>2</sup>*Photonics and Electronics Science and Engineering Center (PESEC), Kyoto University, A1-303 Kyotodaigaku-katsura, Nishikyo, Kyoto 615-8510, Japan*

(Received 19 September 2008; accepted 27 October 2008; published online 13 November 2008)

The N<sub>2</sub>O-grown SiO<sub>2</sub>/4H-SiC (0001), (033̄8), and (112̄0) interface properties in *p*-channel metal-oxide-semiconductor field-effect transistors (MOSFETs) have been characterized by using gate-controlled diodes. Although the inversion layer is not formed in simple SiC MOS capacitors at room temperature due to its large bandgap, a standard low frequency capacitance-voltage (*C*-*V*) curve can be obtained for the gate-controlled diodes, owing to the supply of minority carriers from the source region. From the quasistatic *C*-*V* curves measured by using gate-controlled diodes, the interface state density has been evaluated by an original method proposed in this study. The interface state density near the valence band edge evaluated by the method is the lowest at the oxides/4H-SiC (033̄8) interface. Comparison with the channel mobility is also discussed. © 2008 American Institute of Physics. [DOI: 10.1063/1.3028016]

The wide bandgap semiconductor silicon carbide (SiC) has superior properties such as high breakdown field, high thermal conductivity, and high saturation electron drift velocity.<sup>1</sup> 4H-SiC metal-oxide-semiconductor field-effect transistors (MOSFETs) have been regarded as a candidate for high-power, high-temperature, and high-speed switches,<sup>2</sup> and several high-voltage 4H-SiC MOSFETs, which outperform Si power devices, have been already reported.<sup>3–5</sup>

In the last decade, the characteristics of SiC MOS devices have been significantly improved through the development of process technology. For example, the usage of 4H-SiC (033̄8)<sup>6</sup> and (112̄0) faces<sup>7</sup> and the utilization of deposited insulators<sup>8–10</sup> are effective to improve the characteristics of SiC *n*-channel MOSFETs. In addition, the nitridation of gate oxides<sup>11–13</sup> is widely adopted to reduce the interface state density near the conduction band edge, leading to high channel mobility in SiC *n*-channel MOS devices.<sup>14</sup> Although the understanding on *n*-channel MOS devices has shown gradual progress, the fundamental study on SiC *p*-channel MOS devices has been lacking. The understanding on SiC MOS interface properties in the lower half of bandgap can contribute to the improvement of SiC power devices and circuits.

Although several groups have reported the *p*-channel MOSFETs on the 4H-SiC (0001) face,<sup>15–17</sup> the crystal face dependences of the interface state density and channel mobility have been still missing. The authors characterized the N<sub>2</sub>O-grown oxides/4H-SiC (0001), (033̄8), and (112̄0) interface properties by using MOSFET structure, called a gate-controlled diode.<sup>18</sup> In the gate-controlled diodes, the capacitance-voltage (*C*-*V*) characteristics were measured between the gate electrode and other electrodes (source, drain, and substrate electrodes) of the MOSFETs. The measured low-frequency *C*-*V* curves demonstrate not “accumulation-depletion-deep depletion” characteristics but “accumulation-

depletion-inversion” characteristics in contrast to the simple SiC MOS capacitors because the source/drain regions act as an external source of holes. By using gate-controlled diodes, the correlation between channel mobility and shallow interface state density has been demonstrated for *n*-channel SiC (0001) MOSFETs.<sup>19</sup> In this study, the authors propose an original method to estimate the interface state density, and the shallow states in the lower half of the bandgap at the SiO<sub>2</sub>/SiC interface are evaluated from the measured *C*-*V* curves obtained by using the gate-controlled diodes.

The *p*-channel MOSFETs were fabricated on *n*-type 4H-SiC 8° off-axis (0001), on-axis (033̄8), and on-axis (112̄0) epilayers. The donor concentration of the *n*-type epilayers was 1 × 10<sup>16</sup>, 5 × 10<sup>16</sup>, and 5 × 10<sup>14</sup> cm<sup>-3</sup> for (0001), (033̄8), and (112̄0) faces, respectively. The 0.3 μm deep source/drain regions were formed by high-dose Al<sup>+</sup> implantation (energy: 10–160 keV; total dose: 5 × 10<sup>15</sup> cm<sup>-2</sup>) at 300 °C. After ion implantation, thermal annealing was carried out at 1700 °C for 20 min with a carbon cap to suppress surface roughening.<sup>20</sup> Thermal oxidation was performed in dry N<sub>2</sub>O ambient (10% diluted in N<sub>2</sub>) at 1300 °C.<sup>13,21</sup> The thickness of gate oxides was 49, 44, and 52 nm for (0001), (033̄8), and (112̄0) faces, respectively. The source/drain and substrate electrodes were Ti/Al/Ni and Ni, respectively, and these electrodes were annealed at 950 °C for 5 min. The gate electrode was Al. The typical channel length (*L*) and width (*W*) were 100 and 200 μm, respectively. The design of long-channel MOSFETs was adopted to minimize the influence of source/drain contact resistance and to suppress short-channel effects.<sup>22</sup> The field-effect mobility of the *p*-channel MOSFETs fabricated on (0001), (033̄8), and (112̄0) faces was 7, 11, and 17 cm<sup>2</sup>/V s, respectively (not shown). The *p*-channel SiC MOSFETs on the (033̄8) and (112̄0) faces exhibit higher channel mobility than that on the (0001) face as is the case for *n*-channel SiC MOSFETs.<sup>6,7</sup>

<sup>a)</sup>Electronic mail: noborio@semicon.kuee.kyoto-u.ac.jp. Tel.: +81-75-383-2302. FAX: +81-75-383-2303.

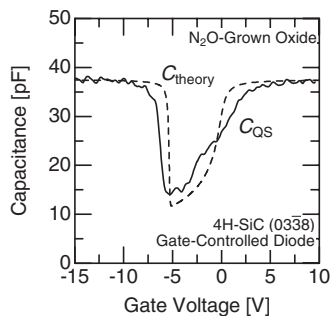


FIG. 1. Quasistatic  $C$ - $V$  curve obtained in  $p$ -channel MOSFETs on the 4H-SiC (0001) face by using a gate-controlled diode. A theoretical  $C$ - $V$  curve is also shown by a dashed line.

Quasistatic  $C$ - $V$  characteristics ( $C_{QS}$ ) were measured at room temperature under dark condition by using the gate-controlled diodes to evaluate the interface state density. The typical sweep rate for the  $C$ - $V$  measurements was about 0.15 V/s. The area of gate electrode is about  $4.9 \times 10^{-4} \text{ cm}^2$ . Figure 1 shows the quasistatic  $C$ - $V$  curve obtained from the (0001) MOSFETs and theoretical low-frequency  $C$ - $V$  curve. The measured  $C$ - $V$  characteristics indicate that the MOS interface under the gate electrode shows strong inversion at sufficiently negative gate voltage, owing to the supply of minority carriers (holes) from the source region. From the measured  $C$ - $V$  curves, the authors evaluated the interface state density near the valence band edge. At first, the surface potential ( $\Psi_S$ )-gate voltage ( $V_G$ ) characteristics were calculated by using the following equation:<sup>23</sup>

$$\Psi_S(V_{G2}) = \int_{V_{G1}}^{V_{G2}} \left[ 1 - \frac{C_{QS}(V_G)}{C_{ox}} \right] dV_G + \Psi_S(V_{G1}). \quad (1)$$

In Eq. (1), in order to determine the absolute value of surface potential, the basis of surface potential must be defined. In this study, the authors assumed that the surface potential calculated from the measured  $C$ - $V$  characteristics coincides with that theoretically obtained at a gate voltage of  $-15 \text{ V}$ . Then, the  $\Psi_S$ - $V_G$  characteristics experimentally obtained are compared with the theoretical  $\Psi_S$ - $V_G$  relationship.

Figures 2(a)–2(c) show the  $\Psi_S$ - $V_G$  curves experimentally and theoretically obtained for the (0001), (0038), and (1120) gate-controlled diodes, respectively. Compared with the theoretical curves, the shift in experimental  $\Psi_S$ - $V_G$  curves toward the negative gate voltage direction is caused by the presence of effective fixed charge (positive) located at the  $\text{SiO}_2/\text{SiC}$  interface and the stretch out of  $\Psi_S$ - $V_G$  curves by the presence of interface states. In the ideal case (theoretical  $\Psi_S$ - $V_G$  curve), the change in gate voltage directly causes that of the surface potential. On the other hand, in the case of the experimental  $\Psi_S$ - $V_G$  curves, the additional increment in gate voltage is needed in order to fill the interface states with holes. Thus, the interface state density ( $D_{it}$ ) can be evaluated from the difference between the slope of  $\Psi_S$ - $V_G$  characteristics theoretically and experimentally obtained as described in the following equation:

$$D_{it} = \frac{C_{ox}}{q} \left( \left. \frac{dV_G}{d\Psi_S} \right|_{\text{theory}} - \left. \frac{dV_G}{d\Psi_S} \right|_{\text{experiment}} \right). \quad (2)$$

From this equation, the interface state density near the valence band edge in the  $p$ -channel SiC MOSFETs was calculated. This method can be also used to estimate the interface

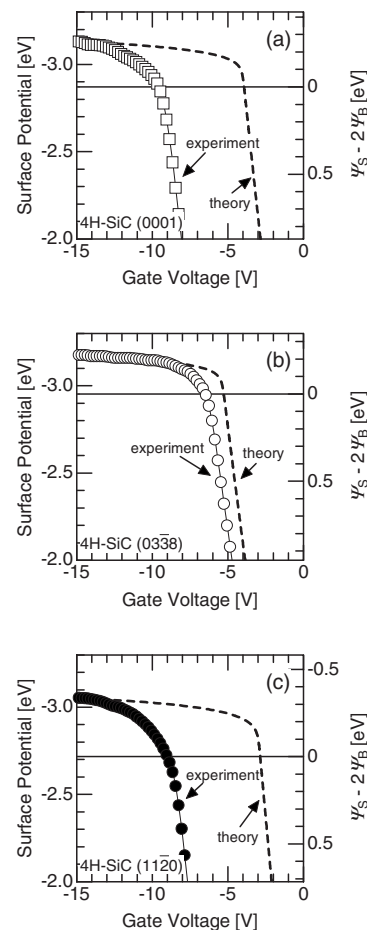


FIG. 2.  $\Psi_S$ - $V_G$  characteristics of the fabricated MOSFETs on (a) (0001), (b) (0038), and (c) (1120) faces. Open squares in (a), open circles in (b), and closed circles in (c) mean the  $\Psi_S$ - $V_G$  characteristics experimentally obtained. Dashed line means the theoretical  $\Psi_S$ - $V_G$  curve. The right vertical axis denotes the  $\Psi_S - 2\Psi_B$  and the solid line represents the  $\Psi_S = 2\Psi_B$  (onset of strong inversion).

state density near the conduction band edge in the  $n$ -channel MOSFETs.

Figure 3 shows the distributions of the interface state density near the valence band edge in the (0001), (0038), and (1120) MOSFETs. From Fig. 3, the interface state density is exponentially increased toward the valence band edge and reaches  $2 \times 10^{12} \text{ cm}^{-2} \text{ eV}^{-1}$  at  $E_V + 0.2 \text{ eV}$  for the (0001) interface. On the other hand, the (0038) face shows a lower interface state density of  $1 \times 10^{12} \text{ cm}^{-2} \text{ eV}^{-1}$  at 0.2 eV above

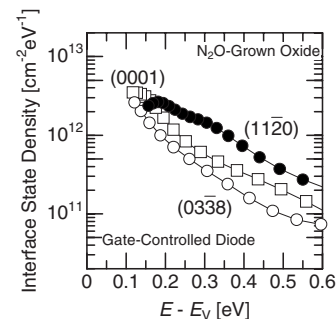


FIG. 3. Distribution of interface state density on the 4H-SiC (0001) face (open squares), (0038) face (open circles), and (1120) face (closed circles). The interface state density was estimated by  $C$ - $V$  curves measured by using the gate-controlled diode structure.

the valence band edge. Contrary to expectations, the (11 $\bar{2}$ 0) face exhibits higher interface state density than the (03 $\bar{3}$ 8) face, and the interface state density is  $2 \times 10^{12} \text{ cm}^{-2} \text{ eV}^{-1}$  at  $E_V + 0.2 \text{ eV}$ . Compared with the SiO<sub>2</sub>/4H-SiC (0001) interface, the interface state density at the SiO<sub>2</sub>/4H-SiC (11 $\bar{2}$ 0) interface is high in the deep energy region and relatively low in the shallow energy region from the valence band edge.

The gate voltage at which the MOS interface becomes strong inversion can be obtained from the intersection of  $\Psi_S - V_G$  curve and  $\Psi_S = 2\Psi_B$  line (horizontal solid line in Fig. 2). The effective fixed charge at the MOS interface was calculated from the difference between the theoretical and experimental gate voltage at which the MOS interface becomes strong inversion. A highest effective fixed charge (positive) of  $3.0 \times 10^{12} \text{ cm}^{-2}$  was obtained for the (11 $\bar{2}$ 0) face, and the effective fixed charge was lowest at the (03 $\bar{3}$ 8) interface ( $4.6 \times 10^{11} \text{ cm}^{-2}$ ). The effective fixed charge at the (0001) interface was  $2.5 \times 10^{12} \text{ cm}^{-2}$ . The magnitude of the effective fixed charge is consistent with that of the interface state density in the deep energy region from the valence band edge as shown in Fig. 3. The high effective fixed charge at the (11 $\bar{2}$ 0) interface may be mainly due to the high density of interface state in the deep energy region.

The N<sub>2</sub>O-grown oxide/4H-SiC (03 $\bar{3}$ 8) interface exhibits the lowest interface state density, leading to the high channel mobility in the (03 $\bar{3}$ 8) MOSFETs. Although the N<sub>2</sub>O-grown oxides/4H-SiC (11 $\bar{2}$ 0) interface shows high interface state density in the deep energy region, the *p*-channel MOSFETs on 4H-SiC (11 $\bar{2}$ 0) face exhibit high channel mobility as described above. The main reason for the high channel mobility in the (11 $\bar{2}$ 0) MOSFETs may be the low donor concentration ( $N_D = 5 \times 10^{14} \text{ cm}^{-3}$ ) of the employed epilayers. The channel mobility of MOSFETs generally depends on the doping concentration of epilayers.<sup>21,24</sup> The decrease in donor concentration results in an increase in channel mobility because the influence of surface roughness scattering and Coulomb scattering from the charges located near the interface is weakened due to its low vertical electric field in the inversion layer. Although the high effective fixed charge density was observed in the (11 $\bar{2}$ 0) MOSFETs as mentioned above, the charges hardly affected the channel mobility of the MOSFETs due to small effect of Coulomb scattering. The low donor concentration contributes to the high channel mobility in the (11 $\bar{2}$ 0) MOSFETs. In addition, the SiO<sub>2</sub>/4H-SiC (11 $\bar{2}$ 0) interface shows the relatively low interface state density near the valence band edge. In the case of 4H-SiC *n*-channel MOSFETs, the interface state density near the conduction band edge adversely affects the channel mobility due to severe electron trapping.<sup>14</sup> In a similar way, the channel mobility of *p*-channel MOSFETs fabricated on the (0001) face may be severely influenced by the shallow interface states, which cause hole trapping. This relatively low density of interface states also contributes to the increase in channel mobility in (11 $\bar{2}$ 0) face.

In conclusion, the authors have investigated the correlation between the characteristics of *p*-channel 4H-SiC MOSFETs with N<sub>2</sub>O-grown oxides and their interface prop-

erties. The fabricated *p*-channel MOSFETs exhibited a channel mobility of  $7 \text{ cm}^2/\text{V s}$  for the (0001) face,  $11 \text{ cm}^2/\text{V s}$  for the (03 $\bar{3}$ 8) face, and  $17 \text{ cm}^2/\text{V s}$  for the (11 $\bar{2}$ 0) face. The shallow interface state density was estimated from the  $\Psi_S - V_G$  characteristics calculated by using the quasistatic and theoretical low-frequency *C-V* curves of the gate-controlled diodes. The SiO<sub>2</sub>/4H-SiC (03 $\bar{3}$ 8) interface exhibited the lowest interface state density ( $D_{it} = 1 \times 10^{12} \text{ cm}^{-2} \text{ eV}^{-1}$  at  $E_V + 0.2 \text{ eV}$ ). The high channel mobility in the (11 $\bar{2}$ 0) MOSFETs may be attributed to the low doping concentration in *n*-type epilayer and relatively low interface state density near the valence band edge. The usage of the nonbasal faces and the nitridation of gate oxides are attractive methods to enhance the characteristics of both 4H-SiC *p*-channel and *n*-channel MOS-based devices.

This work was supported in part by a Grant-in-Aid for Research Fellow (for M.N.) and for Scientific Research (Grant No. 18206032) from the Japan Society for the Promotion of Science and by Global COE Program (C09) from the Ministry of Education, Culture, Sports, Science, and Technology, Japan.

<sup>1</sup>H. Matsunami and T. Kimoto, *Mater. Sci. Eng., R.* **20**, 125 (1997).

<sup>2</sup>J. A. Cooper, Jr., M. R. Melloch, R. Singh, A. Agarwal, and J. W. Palmour, *IEEE Trans. Electron Devices* **49**, 658 (2002).

<sup>3</sup>D. Peters, R. Schörner, P. Friedrichs, and D. Stephani, *Mater. Sci. Forum* **433-436**, 769 (2003).

<sup>4</sup>M. Marin, A. Saha, and J. A. Cooper, *IEEE Trans. Electron Devices* **51**, 1721 (2004).

<sup>5</sup>M. Noborio, J. Suda, and T. Kimoto, *IEEE Trans. Electron Devices* **54**, 1216 (2007).

<sup>6</sup>T. Hirao, H. Yano, T. Kimoto, H. Matsunami, and H. Shiomi, *Mater. Sci. Forum* **389-393**, 1065 (2002).

<sup>7</sup>H. Yano, T. Hirao, T. Kimoto, H. Matsunami, K. Asano, and Y. Sugawara, *IEEE Electron Device Lett.* **20**, 611 (1999).

<sup>8</sup>T. Kimoto, H. Kawano, M. Noborio, J. Suda, and H. Matsunami, *Mater. Sci. Forum* **527-529**, 987 (2006).

<sup>9</sup>S. Hino, T. Hatayama, J. Kato, E. Tokumitsu, N. Miura, and T. Oomori, *Appl. Phys. Lett.* **92**, 183503 (2008).

<sup>10</sup>M. Noborio, J. Suda, and T. Kimoto, *IEEE Trans. Electron Devices* **55**, 2054 (2008).

<sup>11</sup>P. Jamet, S. Dimitrijević, and P. Tanner, *J. Appl. Phys.* **90**, 5058 (2001).

<sup>12</sup>G. Y. Chung, C. C. Tin, J. R. Williams, K. McDonald, R. K. Chanana, R. A. Weller, S. T. Pantelides, L. C. Feldman, O. W. Holland, M. K. Das, and J. W. Palmour, *IEEE Electron Device Lett.* **22**, 176 (2001).

<sup>13</sup>L. A. Lipkin, M. K. Das, and J. W. Palmour, *Mater. Sci. Forum* **389-393**, 985 (2002).

<sup>14</sup>N. S. Saks, *Silicon Carbide - Recent Major Advances*, edited by W. J. Choyke, H. Matsunami, and G. Pensl (Springer, Berlin, 2003) 387.

<sup>15</sup>J. S. Han, K. Y. Cheong, S. Dimitrijević, M. Laube, and G. Pensl, *Mater. Sci. Forum* **457-460**, 1401 (2004).

<sup>16</sup>M. Okamoto, M. Tanaka, T. Yatsuo, and K. Fukuda, *Appl. Phys. Lett.* **89**, 023502 (2006).

<sup>17</sup>M. K. Das, S. K. Haney, C. Jonas, and Q. Zhang, *Mater. Sci. Forum* **556-557**, 667 (2007).

<sup>18</sup>A. S. Grove and D. J. Fitzgerald, *Solid-State Electron.* **9**, 783 (1966).

<sup>19</sup>S. Suzuki, S. Harada, R. Kosugi, J. Senzaki, W. Cho, and K. Fukuda, *J. Appl. Phys.* **92**, 6230 (2002).

<sup>20</sup>Y. Negoro, K. Katsumoto, T. Kimoto, and H. Matsunami, *J. Appl. Phys.* **96**, 224 (2004).

<sup>21</sup>T. Kimoto, Y. Kanzaki, M. Noborio, H. Kawano, and H. Matsunami, *Jpn. J. Appl. Phys., Part 1* **44**, 1213 (2005).

<sup>22</sup>M. Noborio, Y. Kanzaki, J. Suda, and T. Kimoto, *IEEE Trans. Electron Devices* **52**, 1954 (2005).

<sup>23</sup>C. N. Berglund, *IEEE Trans. Electron Devices* **13**, 701 (1966).

<sup>24</sup>S. Takagi, A. Toriumi, M. Iwase, and H. Tango, *IEEE Trans. Electron Devices* **41**, 2357 (1994).